Materials Transactions, Vol. 61, No. 2 (2020) pp. 381 to 386

Analysis of Bone Regeneration Based on the Relationship between the Orientations of Collagen and Apatite in Mouse Femur

Ryosuke Ozasa[1], Mayuko Nakatsu[1,*1], Atsushi Moriguchi[1,*1], Kyohei Sasaki[1,*1], Takuya Ishimoto[1], Masahiro Okada[2], Takuya Matsumoto[2] and Takayoshi Nakano[1,*2]

[1]*Division of Materials and Manufacturing Science, Graduate School of Engineering, Osaka University, Suita 565-0871, Japan*
[2]*Department of Biomaterials, Okayama University, Graduate School of Medicine, Dentistry and Pharmaceutical Sciences, Okayama 700-8558, Japan*

In this study, we focused on the preferential orientation of the extracellular matrix (ECM) of bone, since ECM orientation has been shown to significantly affect the mechanical functions of bones. Bone analysis is in most cases based on the premise that the apatite crystallizes on the collagen template such that its *c*-axis is parallel with the running direction of the collagen fibril. Bone regeneration analysis has also been discussed assuming that the apatite *c*-axis orientation reflects collagen orientation. To understand the regeneration processes of both collagen and apatite individually, the preferential orientations of apatite and collagen in regenerated bone were simultaneously analyzed using a bone regeneration model of mouse femur with an 0.8-mm drill hole defect. The defects in mouse femur were filled with mineralized bone matrix, which shows an intact mineral density. However, the directions of orientation of the collagen and apatite deviate from the femur longitudinal axis in the regenerated bone. Moreover, electron diffraction analysis revealed that the apatite *c*-axis aligned along the extended axis of a collagen fibril both in regenerated and intact bones, indicating that the direction of the apatite *c*-axis is regulated by collagen fibril orientation even in the regenerated bone. In conclusion, the less-oriented apatite crystallite observed in the regenerated bone was shown to be formed due to the less-oriented collagen fibrils. [doi:10.2320/matertrans.MT-M2019341]

(Received November 20, 2019; Accepted November 27, 2019; Published December 27, 2019)

Keywords: *collagen orientation, apatite c-axis orientation, bone regeneration*

1. Introduction

Bone tissue has an anisotropic and hierarchical microstructure dominantly composed of collagen and nanoscale apatite crystallite.[1)] One of the main mineral elements of the bone extracellular matrix (ECM), apatite, is an anisotropic material due to its hexagonal structure (e.g., the crystallographic *c*-axis of apatite single crystals is stiffer than the *a*-axis).[2)] Furthermore, one of the main organic elements in bone ECM, collagen, is also an anisotropic material whose axial load capacity is greater than the load capacity along the other axis.[3)] This is attributed to the anisotropic features of tropocollagen molecules lying in the longitudinal fibril direction. In intact bones, apatite *c*-axis aligns almost parallel to the extended collagen fibrils due to the epitaxial crystallization of the apatite on the collagen template through an *in vivo* self-assembly process.[4)] Therefore, ECM microarrangement regulates bone mechanical functions (stiffness and toughness) without a change in bone mass of ECM in an intact bone.[5)]

Primarily, the change in orientation of the apatite *c*-axis has been discussed with respect to the regeneration processes of bone. It was previously revealed that the original apatite texture and Young's modulus synchronously degrade even if bone mass fully recovers.[6,7)] Despite both collagen orientation as well as apatite *c*-axis orientation being crucial to determine bone material integrity, only apatite *c*-axis orientation has been studied on the premise that parallelism between the apatite *c*-axis and collagen running axis materializes in the regenerated bone. Understanding the collagen orientation in regenerated bone is necessary to estimate the recurrent risk of bone injury precisely.

The purpose of the present study is to simultaneously analyze the preferential orientation of apatite and collagen in regenerated bone using a regeneration model of mouse femur with an 0.8-mm drill hole defect.[8)] To address this, bone properties including bone mass, degree of preferential orientation of collagen and apatite *c*-axis, and orientation relationship between collagen fibril and apatite crystallites were analyzed either at several μm- or 100 nm-scales.

2. Experimental Procedure

2.1 Generation of regeneration model of mice

Four 11-week-old male C57BL6 mice were used in this study (Charles River Japan Inc., Kanagawa, Japan). They were kept under conventional conditions, individually housed in plastic cages at 25°C and 55% humidity with a 12-h light/12-h dark cycle, and fed *ad libitum* with a formal diet (CRF-1; Charles River Japan Inc.) and tap water throughout the study. A 0.8-mm drill hole was generated in the anterior cortex of the right femurs at midshaft using a dental drill and the left femurs were sham-operated (control) under anesthesia using an intraperitoneal injection of sodium pentobarbital (Nacalai Tesque co. ltd., Kyoto, Japan) and intramuscular injection of medetomidine (Nippon Zenyaku Kogyo Co., Ltd., Tokyo, Japan). After bone regeneration for four weeks, mice were exposed to isoflurane and perfusion fixation was performed after the measurement of bone weight. All animal procedures and protocols were approved by the Animal Experiment Committee of Osaka University Graduate School of Engineering (approval number: 29-4-0).

2.2 Sample preparation

The bilateral femurs were extracted from mice immediately after sacrifice. Isolated bones from three out of four mice were used for the analysis by peripheral quantitative

*[1]Graduate Student, Osaka University
*[2]Corresponding author, E-mail: nakano@mat.eng.osaka-u.ac.jp

computed tomography (pQCT), microbeam X-ray diffractometer (μ-XRD) system, and birefringence. The bones were immersed in a 10 mass% neutral buffered formalin solution for 1 week and immersed in a 70% ethanol solution until analysis. After analysis via pQCT, the posterior regions of the femurs were ground in wet condition so that the X-ray would penetrate the anterior cortex of femurs during μ-XRD measurements. Then, the bone specimens were ground in wet condition to a thickness of approximately 100 μm for birefringence measurements. The femurs of the remaining mice were used for analysis by transmission electron microscopy (TEM) with a selected area diffraction pattern (SADP). For TEM observation, the bones were cut into small specimens with a microtome (Model 660; South Bay Technology Inc., CA, USA) equipped with a diamond wheel saw (Ted Pella Inc., CA, USA) and treated using modified Karnovsky's fixative solution.[9] The specimens were dehydrated and embedded in epoxy resin. Ultrathin sections (90 nm in thickness) were cut along the frontal plane with a microtome (Leica Ultracut UCT; Leica Biosystems Inc., IL, USA).

2.3 Evaluation of bone regeneration by micro computed tomography (μ-CT)

The defected portions were imaged once in two weeks until sacrifice by μ-CT (R_mCT2; Rigaku Corp., Tokyo, Japan) which was operated at 80 kV and 90 μA with a spatial resolution of $30 \times 30 \times 30\,\mu m^3$. After sampling, cross-sectional images of the cortex of the femurs were imaged by another μ-CT apparatus (SMX-CT100; Shimadzu corp., Kyoto, Japan) which was operated at 46 kV and 90 μA with a resolution of $8.5 \times 8.5 \times 8.5\,\mu m^3$.

2.4 Measurement of bone mineral density by pQCT

Volumetric bone mineral density (vBMD) of the regenerated bone was measured using a pQCT system (XCT Research SA+; Stratec Medizintechnik GmbH, Birkenfeld, Germany). The cross section of the femur at midshaft along the longitudinal axis of the bone was scanned at a resolution of $70 \times 70 \times 260\,\mu m^3$. The vBMD values of all pixels in the region of the regenerated bone and the corresponding region of the intact bone were averaged to obtain the representative value of vBMD in each bone.

2.5 Analysis of apatite *c*-axis orientation of femur along bone longitudinal axis of femur by a μ-XRD system

To assess the degree of preferential orientation of the apatite *c*-axis of the femur along the bone longitudinal axis, X-ray diffraction analysis was performed by a μ-XRD system (R-Axis BQ; Rigaku, Tokyo, Japan) equipped with a transmission-type optical system and an imaging plate (storage phosphors) (FUJIFILM, Tokyo, Japan) placed behind the specimen. Detailed conditions for measurement have been described in the previous paper.[10] In this study, the incident beam focused into a diameter of 300 μm was used to irradiate the anteroposterior axis on the anterior surface of the femur at midshaft. Diffraction data were collected for 900 s. The degree of preferential orientation of the apatite *c*-axis was evaluated by the relative intensity ratio of the (002) diffraction peak to the (310) peak in the X-ray profile. The relative intensity ratio of 0.8 indicates random orientation in this apparatus.

2.6 Analysis of collagen orientation of femur along bone longitudinal axis by birefringence system

To assess the degree of preferential orientation of the collagen of the femur along the bone longitudinal axis, bone specimens were observed by a two-dimensional birefringence measurement system (WPA-micro; Photonic Lattice, Miyagi, Japan) attached to an upright microscope (BX60; Olympus, Tokyo, Japan). Analysis was performed by a WPA-VIEW software (version 2.4.2.9; Photonic Lattice) as previously described.[11,12] As collagen is a positive birefringent material, the direction of the slow axis corresponds to the direction of the collagen fibril.[13] The orientation order parameter f_θ was calculated based on the angle distribution of the collagen against the bone longitudinal axis. f_θ takes a value ranging from -1 (collagen perfectly aligned perpendicular to the longitudinal axis of the femur) to 1 (collagen perfectly aligned parallel to the longitudinal axis of the femur).

2.7 Evaluation of the orientation relationship between the collagen running axis and apatite *c*-axis

To evaluate the orientation relationship between the collagen running axis and apatite *c*-axis, TEM with SADP (JEOL-2100F; JEOL Ltd., Tokyo, Japan) at an acceleration voltage of 200 kV was used. SADP analyses were performed for regions approximately 1500 nm and 150 nm in diameter using a selector aperture. The intensity distribution of the (002) peaks was azimuthally quantified using a software (iTEM; Olympus, Tokyo, Japan). The data was fitted with a Gaussian-based function by using Igol Pro8.0 (WaveMetrics, OR, USA). The full width at half maximum (FWHM) was calculated to evaluate the degree of preferential orientation along the analysis axis.

2.8 Statistical analysis

The data were averaged and represented as mean $\pm$ standard deviation (SD). Statistical comparisons between the two means were performed using a two-tailed unpaired Student's *t*-test followed by a F-test for homoscedasticity. $P < 0.05$ was considered significant.

3. Results and Discussions

3.1 Bone mass in regenerated bone

In the present mice model, a hole defect with a diameter of 0.8 mm was introduced in the femoral cortex at midshaft. The defects neither resulted in a bone fracture nor disturbed the normal walking activity of mice. The experimental mice immediately before sacrifice showed normal body weight (26.0 ± 0.4 g), which is almost the same as the weight curve provided by the supplier. Thus, health conditions of experimental mice were maintained normal in this study.

At the defect, new bone formed over time, and the defect was completely filled with mineralized bone four weeks after operation (Fig. 1(a)). Cross-sectional images of the femurs confirm the reconstruction of the cortical bone in shape (Fig. 1(b)), which is in line with the previous study.[14] Moreover, the regenerated cortical bone shows the same

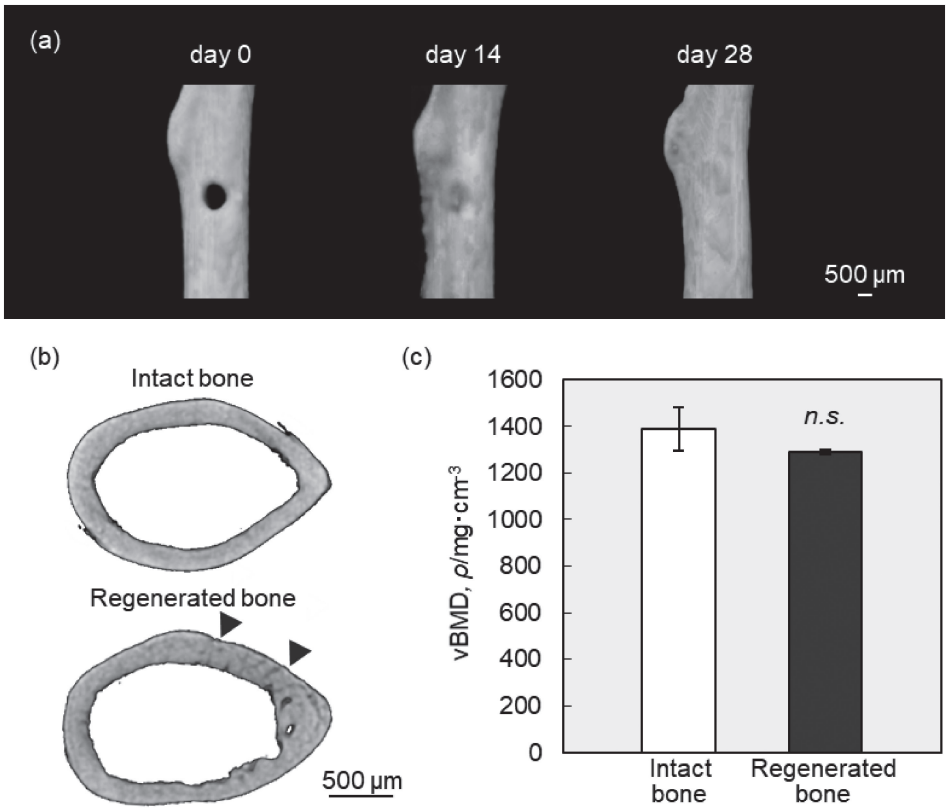

Fig. 1 Spontaneous recovery of bone mass in regenerated femurs of mice. (a) The process of bone regeneration at the defect site and (b) cross-sectional images of intact bone cortex (upper) and regenerated bone cortex (lower) imaged by micro computed tomography (μ-CT). The edges of the defect are indicated by the black arrowheads. (c) Volumetric bone mineral density (vBMD) in intact bone and regenerated bone at the defect site (n = 3). *n.s.*: not significant.

vBMD value as that of intact bone (Fig. 1(c)). Therefore, these results show that bone mass at this defect size is fully recovered without any treatments of the mice model. Mice skeleton exhibits some common features with human skeleton and the knowledge obtained from mice should be considered to be applicable to humans, yet, osteonal remodeling of the cortical bone does not occur in mice.[15] This means that, in mice, once a defect in a bone is formed, it is hardly replaced with a new bone thereafter. This indicates that the bone matrix formed at early stages of bone regeneration is retained as it was constructed throughout the process of bone regeneration. Thus, the regeneration model of mice is the suitable model to investigate the properties of the bone matrix generated at early stages of bone regeneration.

3.2 Deterioration of the microstructures including collagen and apatite in regenerated bone

Bone mass is completely recovered in a regenerated bone (Fig. 1). By contrast, the bone microstructures including the collagen and apatite are notably disrupted (Fig. 2). In an intact bone, collagen aligns uniformly along the bone's longitudinal axis, however, collagen loses its normal alignment in the regenerated bone (Figs. 2(a), (b)). As a result, the degree of collagen orientation along the bone's longitudinal axis statistically decreases in the regenerated bone compared with that in the intact bone (Fig. 2(c)). It is demonstrated that the angle of collagen orientation notably deviates from its original axis in the regenerated bones of mice. Likewise, degree of preferential orientation of the apatite *c*-axis in regenerated bones statistically decreases in regenerated bone compared with that when the bone is intact (Fig. 2(d)). It has been reported that the crystallographic alignment of the apatite *c*-axis degrades in rabbit ulna at early stages of bone regeneration, and it takes a long time to fully recover.[7] Thus, the aberrant orientation of the apatite *c*-axis in original axis is a common characteristic of bone tissue during the early stages of bone regeneration regardless of the animal species.

On the other hand, the degree of apatite *c*-axis orientation shows a positive correlation with the degree of collagen orientation ($R^2 = 0.85$, $P = 8.8 \times 10^{-3}$; Fig. 2(e)). This represents that the apatite *c*-axis orientation reflects collagen orientation depending on the orientation degree, indicating a possibility that aberrant orientation of the apatite *c*-axis occurs due to the disturbed collagen orientation because the apatite crystallite is mineralized on the collagen template during bone matrix formation. Hence, nucleation and crystal growth of apatite occur at intrafibrillar or extrafibrillar regions in the hierarchical structure of the collagen fibril.[16] Therefore, microscopic analysis at the scale of the collagen fibril is required in order to confirm the orientation relationship between the axis along which the collagen runs and apatite *c*-axis in the regenerated bone.

3.3 Orientation relationship between collagen/apatite in regenerated bone

In the TEM analysis, two types of selector apertures were

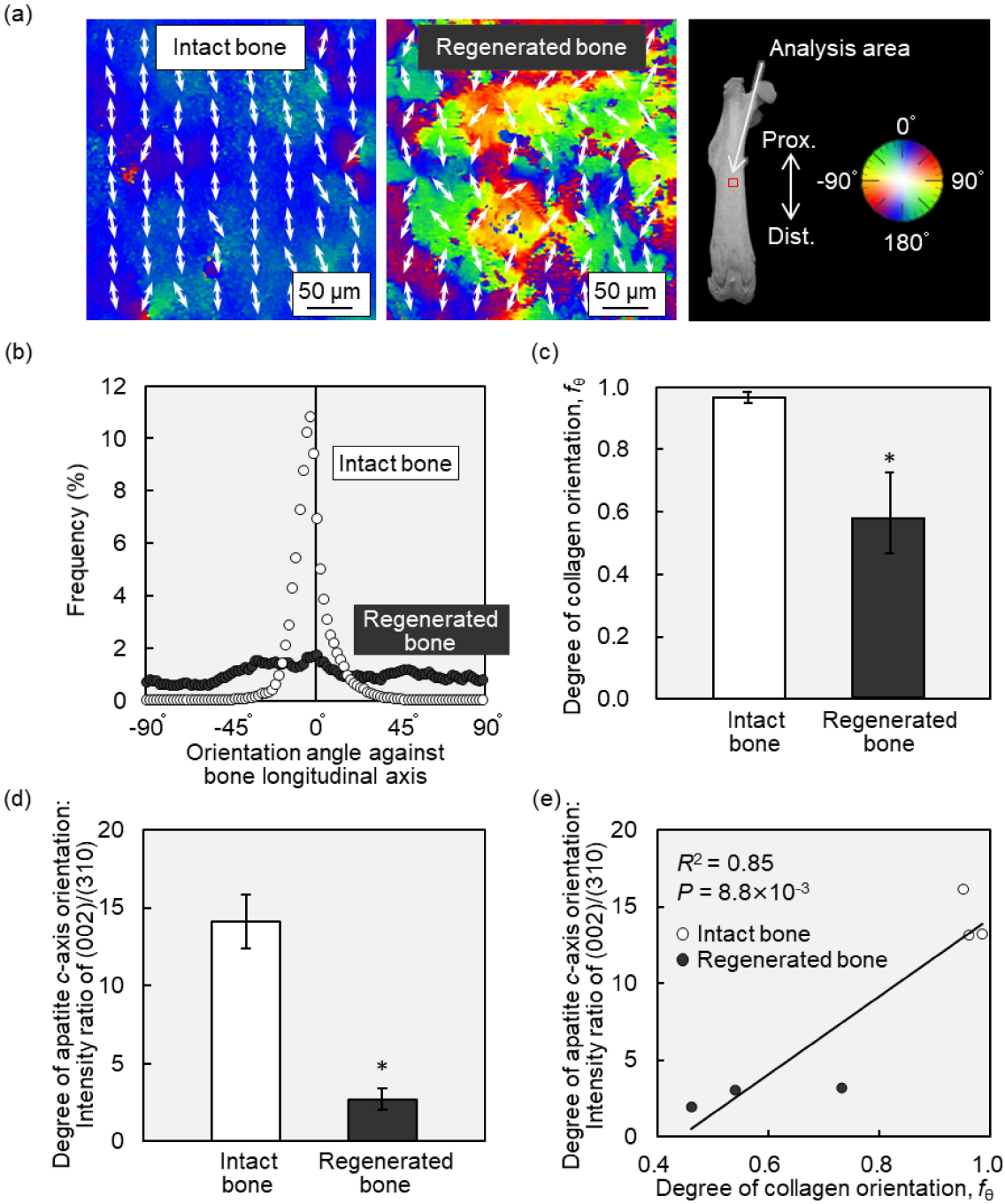

Fig. 2 Deviation of the orientations of collagen and apatite crystallites from the bone longitudinal axis in mouse regenerated femur. (a) Color mapping images, where color and arrows indicate the orientation angle of collagen against the long bone axis (0°), and (b) histograms of collagen orientation. Quantitative comparison of (c) degree of collagen orientation and (d) apatite *c*-axis orientation along the bone longitudinal axis between intact bone and regenerated bone (n = 3). (e) Correlation between the degree of collagen orientation and that of apatite *c*-axis. ∗: $P < 0.05$.

used, based on the purpose; one to evaluate the deviation of apatite *c*-axis orientation from the bone longitudinal axis (microscale), and the other to evaluate that from the collagen fibril running axis (nanoscale). The diameter of one collagen fibril is reported to be 30–300 nm[17] (Fig. 3(a)) and thus, SADP analysis was carried out with the appropriate selector aperture to obtain diffraction data from apatite crystallites.

Figure 3 shows the bright-field images and the electron diffraction patterns of intact and regenerated bones. Microscale analysis reveals that apatite crystallites on the collagen fibril show a clear and narrow arc of the (002) peak, which corresponds to the *c*-axis of apatite, in intact bone (Fig. 3(c); FWHM = 36.4), whereas that of regenerated bone scatters (Fig. 3(e); FWHM = 48.5). These results are consistent with results obtained from μ-XRD analysis (Fig. 2(d)). On the other hand, nanoscale analysis shows alternating hole and overlap regions (abbreviated as H and O, respectively in Figs. 3(a), (f), (h)) in collagen, with a characteristic D period of approximately 67 nm,[17] which indicates the direction of collagen fibril orientation (Fig. 3(f), (h)). Here, the direction of maximum intensity of the arc of (002) peak approximately corresponds to the collagen running axis both in intact

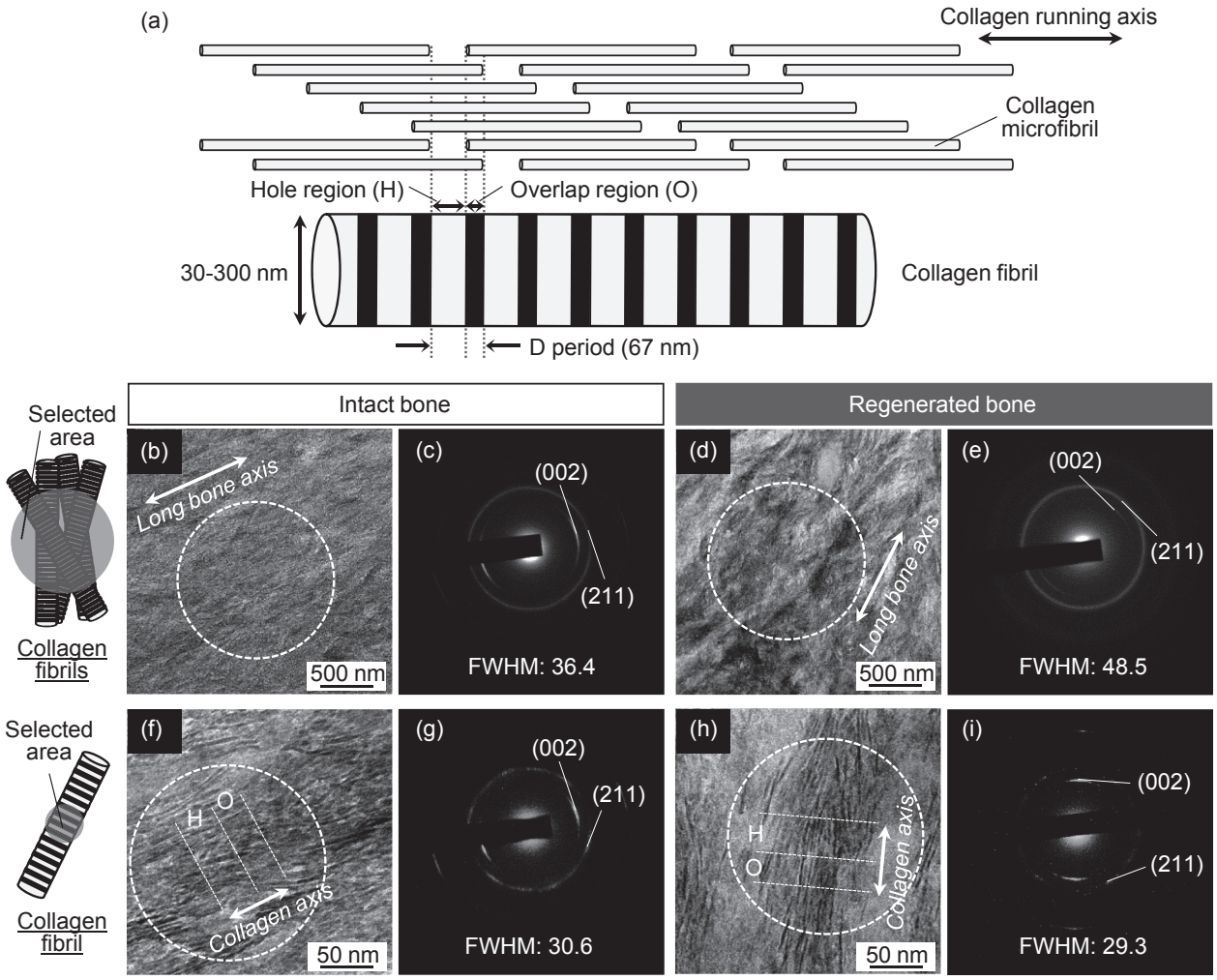

Fig. 3 Orientation relationship between collagen and apatite crystallites in regenerated bone. (a) A schematic illustration of D period repeating within collagen fibril composed of staggered array of collagen microfibrils. Bright-field images of (b) intact and (d) regenerated bones at 10 K magnification, and (f) intact and (h) regenerated bones at 100 K magnification observed by transmission electron microscopy. (c), (e), (g), (i) The selected area diffraction pattern analysis for regions surrounded by dotted lines in (b), (d), (f), (h). H: hole region, O: overlap region.

(Figs. 3(f), (g)) and regenerated bones (Figs. 3(h), (i)). Besides, FWHM value in regenerated bone (29.3) is comparable to that of intact bone (30.6). This suggests that the apatite *c*-axis is regulated by collagen fibrils even in the regenerated bone. Given that collagen disrupts the original orientation in regenerated bone (Figs. 2(a)–(c)), the deterioration of apatite *c*-axis orientation against the longitudinal axis of the femur in regenerated bone is attributed to the deviation of collagen orientation from the bone longitudinal axis, since epitaxial orientation of apatite *c*-axis against the collagen template is maintained even in regenerated bone, as revealed in this study.

When evaluating the apatite *c*-axis orientation by SADP, kinetic effect cannot be excluded. The difference in the net amount of apatite at the analysis region of each specimen causes difference in kinetic effects between analyses. For minimizing this, the same thickness of ultrathin bone specimens (90 nm) were prepared using the microtome technique, because mineral density was the same regardless of the experimental group (Fig. 1(c)).

All evaluation methods used in this study were invasive. A method using ultrasonic waves has been proposed for noninvasive bone analysis,[18] which is important in clinical settings. As ultrasound utilizes elastic waves, the ultrasonic velocity reflects the elastic properties of the propagating material. Therefore, ultrasonic velocity dominantly reflects the property of the stiffer apatite. However, the orientation of collagen is also an important index for determining bone toughness,[19] which is one of the important mechanical properties of bones reflecting fracture risk. In regenerative bone, it has become clear that the orientation of collagen and apatite is synchronized, so there is a possibility that ultrasonic velocity can be used for non-invasive evaluation of not only elastic properties, but also toughness. This correspondence between collagen orientation and apatite orientation has been also observed in osteopetrotic bone,[10] osteoporotic bone,[20] cancer metastatic bone,[21,22] osteogenesis imperfecta,[23] and bone exposed to reduced load.[24] It is very beneficial clinically that non-invasive collagen analysis can be applied to such diseased or abnormal bones.

The findings obtained in this study also indicate potential methodologies that can be used for bone regeneration. It is important to establish a method that targets the orientation of collagen in order to finally obtain regenerated bone with

appropriate orientation of both apatite and collagen and excellent mechanical functions. The arrangement of osteoblasts that produce collagen in a specific direction[25–27] is a promising factor influencing rapid recovery of the regenerative bone microstructure and function.

4. Conclusion

In this study, we simultaneously analyzed the preferential orientation of apatite and that of collagen in the mouse regenerated bone using μ-XRD, birefringence, and electron diffraction analyses. Although the apatite *c*-axis corresponded well with the collagen running direction both in the intact and regenerated bones, the recovery in the orientation of the apatite *c*-axis and collagen fibrils were both impaired. This demonstrates that the direction of apatite *c*-axis is regulated by collagen fibril orientation, even in regenerated bone. The findings obtained here suggest that the strategy for bone regeneration should focus on the reconstruction of collagen orientation, as a crystallographic template of apatite crystallization.

Acknowledgments

This work was funded by the Grants-in-Aid for Scientific Research (Grant Nos. JP18H05254, JP18H03844, and JP17H06224) from the Japan Society for the Promotion of Science (JSPS).

REFERENCES

1) H.D. Wagner and S. Weiner: J. Biomech. **25** (1992) 1311–1320.
2) B. Viswanath, R. Raghavan, U. Ramamurty and N. Ravishankar: Scr. Mater. **57** (2007) 361–364.
3) M.P.E. Wenger, L. Bozec, M.A. Horton and P. Mesquida: Biophys. J. **93** (2007) 1255–1263.
4) W.J. Landis, K.J. Hodgens, J. Arena, M.J. Song and B.F. McEwen: Microsc. Res. Tech. **33** (1996) 192–202.
5) T. Nakano, K. Kaibara, Y. Tabata, N. Nagata, S. Enomoto, E. Marukawa and Y. Umakoshi: Bone **31** (2002) 479–487.
6) T. Nakano, K. Kaibara, T. Ishimoto, Y. Tabata and Y. Umakoshi: Bone **51** (2012) 741–747.
7) T. Ishimoto, T. Nakano, Y. Umakoshi, M. Yamamoto and Y. Tabata: J. Bone Miner. Res. **28** (2013) 1170–1179.
8) Y.P. Zhao, Q.Y. Tian, S. Frenkel and C.J. Liu: Biomaterials **34** (2013) 6412–6421.
9) L.M. McNamara, R.J. Majeska, S. Weinbaum, V. Friedrich and M.B. Schaffler: Anat. Rec. **292** (2009) 355–363.
10) T. Ishimoto, B. Sato, J.-W. Lee and T. Nakano: Bone **103** (2017) 216–223.
11) R. Ozasa, A. Matsugaki, Y. Isobe, T. Saku, H.S. Yun and T. Nakano: J. Biomed. Mater. Res. A **106** (2018) 360–369.
12) T. Ishimoto, K. Yamada, H. Takahashi, M. Takahata, M. Ito, T. Hanawa and T. Nakano: Bone **108** (2018) 25–33.
13) N.M. Kalwani, C.A. Ong, A.C. Lysaght, S.J. Haward, G.H. McKinley and K.M. Stankovic: J. Biomed. Opt. **18** (2013) 026021.
14) Y.-X. He, G. Zhang, X.-H. Pan, Z. Liu, L.-Z. Zheng, C.-W. Chan, K.-M. Lee, Y.-P. Cao, G. Li, L. Wei, L.-K. Hung, K.-S. Leung and L. Qin: Bone **48** (2011) 1388–1400.
15) R.L. Jilka: J. Gerontol. A **68** (2013) 1209–1217.
16) D. Kim, B. Lee, S. Thomopoulos and Y.S. Jun: Nat. Commun. **9** (2018) 962.
17) B.R. Williams, R.A. Gelman, D.C. Poppke and K. Piez: J. Biol. Chem. **253** (1978) 6578–6585.
18) T. Ishimoto, R. Suetoshi, D. Cretin, K. Hagihara, J. Hashimoto, A. Kobayashi and T. Nakano: Bone **127** (2019) 82–90.
19) X. Wang, X. Shen, X. Li and C. Mauli Agrawal: Bone **31** (2002) 1–7.
20) R. Ozasa, T. Ishimoto, S. Miyabe, J. Hashimoto, M. Hirao, H. Yoshikawa and T. Nakano: Calcif. Tissue Int. **104** (2019) 449–460.
21) A. Sekita, A. Matsugaki, T. Ishimoto and T. Nakano: J. Struct. Biol. **197** (2017) 260–270.
22) A. Sekita, A. Matsugaki and T. Nakano: Bone **97** (2017) 83–93.
23) M. Raghavan, N.D. Sahar, R.H. Wilson, M.A. Mycek, N. Pleshko, D.H. Kohn and M.D. Morris: J. Biomed. Opt. **15** (2010) 037001.
24) J. Wang, T. Ishimoto and T. Nakano: Calcif. Tissue Int. **100** (2017) 87–94.
25) A. Matsugaki, N. Fujiwara and T. Nakano: Acta Mater. **9** (2013) 7227–7235.
26) R. Ozasa, A. Matsugaki, Y. Isobe, T. Saku and T. Nakano: Mater. Trans. **58** (2017) 958–962.
27) Y. Nakanishi, A. Matsugaki, K. Kawahara, T. Ninomiya, H. Sawada and T. Nakano: Biomaterials **209** (2019) 103–110.